The Journal of Experimental Biology 212, 1212-1224
Published by The Company of Biologists 2009
doi:10.1242/jeb.026872

Amplitude and frequency modulation control of sound production in a mechanical model of the avian syrinx

Coen P. H. Elemans[1,2,*], Mees Muller[1], Ole Næsbye Larsen[2] and Johan L. van Leeuwen[1]

[1]Experimental Zoology Group, Wageningen University, Marijkeweg 40, NL-6709 PG Wageningen, The Netherlands and [2]Institute of Biology, University of Southern Denmark, Campusvej 55, DK-5230 Odense M, Denmark

*Author for correspondence (e-mail: coen@biology.sdu.dk)

Accepted 30 January 2009

SUMMARY

Birdsong has developed into one of the important models for motor control of learned behaviour and shows many parallels with speech acquisition in humans. However, there are several experimental limitations to studying the vocal organ – the syrinx – *in vivo*. The multidisciplinary approach of combining experimental data and mathematical modelling has greatly improved the understanding of neural control and peripheral motor dynamics of sound generation in birds. Here, we present a simple mechanical model of the syrinx that facilitates detailed study of vibrations and sound production. Our model resembles the 'starling resistor', a collapsible tube model, and consists of a tube with a single membrane in its casing, suspended in an external pressure chamber and driven by various pressure patterns. With this design, we can separately control 'bronchial' pressure and tension in the oscillating membrane and generate a wide variety of 'syllables' with simple sweeps of the control parameters. We show that the membrane exhibits high frequency, self-sustained oscillations in the audio range (>600 Hz fundamental frequency) using laser Doppler vibrometry, and systematically explore the conditions for sound production of the model in its control space. The fundamental frequency of the sound increases with tension in three membranes with different stiffness and mass. The lower-bound fundamental frequency increases with membrane mass. The membrane vibrations are strongly coupled to the resonance properties of the distal tube, most likely because of its reflective properties to sound waves. Our model is a gross simplification of the complex morphology found in birds, and more closely resembles mathematical models of the syrinx. Our results confirm several assumptions underlying existing mathematical models in a complex geometry.

Key words: bird song, biomechanics, bioacoustics, vocal control.

INTRODUCTION

Birdsong is a widely adopted model for sensorimotor and vocal learning, and demonstrates many parallels with human speech acquisition and production (Doupe and Kuhl, 1999). The unique avian vocal organ, the syrinx, has been recognised as the sound-producing organ for centuries. However, because of the delicacy and the location of the syrinx deep in the body, the biomechanics of sound production at the level of the syrinx remains poorly understood. In humans, the larynx is relatively easy to access and detailed studies on vocal fold movements are available (e.g. Seikel et al., 1997). From this body of literature, we know that the vibratory modes of the vocal folds determine the nature of the radiated sound to a large extent (e.g. Herzel et al., 1994; Herzel et al., 1995; Ishizaka and Flanagan, 1972; Švec et al., 1996; Titze, 2002).

At present, there are several experimental limitations to studying the syrinx system *in vivo*: although progress is being made (e.g. Jensen et al., 2007), imaging at sufficiently high temporal resolution remains an experimental challenge. Invasive techniques that use fibre optics provide direct observations, but have the disadvantage that birds have to be anaesthetized: controlled vocalizations can only be induced with gas injections or brain stimulation (Goller and Larsen, 1997a; Goller and Larsen, 1997b; Larsen and Goller, 2002). Measurements of air sac pressure, flow and electromyography (EMG) have been used successfully in spontaneously vocalising birds (e.g. Suthers, 1990; Goller and Suthers, 1996a; Goller and Suthers, 1996b; Vicario, 1991). These experimental techniques face many challenges, such as accurate sensor calibration, tissue rejection and species suitability, that do not constrain *in vitro* studies (Abs, 1980; Fee et al., 1998; Fee, 2002; Paulsen, 1967; Rüppel, 1933) and mathematical models (Elemans et al., 2008a; Fee et al., 1998; Fletcher, 1988; Gardner et al., 2001; Laje and Mindlin, 2002; Laje and Mindlin, 2005b; Zaccarelli et al., 2006). The recent multi-disciplinary approach of combining experimental data and mathematical modelling has greatly improved the understanding of neural control and peripheral motor dynamics of sound generation in birds (Elemans et al., 2008a; Laje and Mindlin, 2002; Laje and Mindlin, 2005b; Laje et al., 2002; Mindlin et al., 2003). These mathematical models make two assumptions on sound production: (1) the fundamental frequency of labial or membrane vibrations determines the frequency of the produced sound, and (2) tension in the syringeal membranes or labia determines their vibration frequency. Optical measurements on vibrations of the labia in a songbird (hill mynah, *Gracula religiosa*) and the tympaniform membranes of two non-songbirds (pigeon, *Columbia livia*, and cockatiel, *Nymphicus hollandicus*) showed that the fundamental frequency of membrane vibration was close or similar to the radiated sound (Larsen and Goller, 1999). These assumptions are further supported by the experimental observations that fundamental frequency of the produced sound correlates with muscle activity (Elemans et al., 2004; Goller and Suthers, 1996a; Goller and Suthers, 1996b) and/or pressure differences over syringeal membranes (Beckers et al., 2003a; Elemans et al., 2008a). These latter observations can be explained if one assumes that syringeal muscle activity and/or pressure differences over the syringeal membranes

affect the tension of the membranes or labia and therefore the fundamental frequency of the sound. However, no direct measurements of labial or membrane tension exist during sound production.

In addition to analytical and numerical modelling, mechanical models can also facilitate the study of biological phenomena (Koehl, 2006) and have provided increasing insight into complex biomechanical problems such as flight mechanics (e.g. Ellington et al., 1996; Sane and Dickinson, 2002), human speech production (e.g. Ruty et al., 2007; Tack et al., 2006; Van Hirtum et al., 2007) and vocal fold prosthetics design (Tack et al., 2006; de Vries et al., 2000). The first mechanical model of the syrinx to our knowledge was developed by Dürrwang (Dürrwang, 1974), who used it to illustrate the concept of Bernoulli's principle during sound production by flow-induced oscillating structures and to study resonance properties of the trachea. His model consisted of a 1 cm diameter round tube with two bars in the middle to which a rubber membrane was glued (Fig. 1A). Air could flow freely on one side of the membrane, but was blocked on the other side ensuring roughly equal air pressure on both sides and a 'labium-imitation' was mounted on the other side. This model generated sound with the vibrating membrane, but unfortunately, no details on the design, membranes or methodology were presented and Dürrwang himself stated that "The few [model] parameters are either of no importance or so difficult to express in numbers (e.g. the elastic properties of the membrane) that a detailed description of the methodology is not provided". Abs (Abs, 1980) presented the second mechanical model as part of an elegant multidisciplinary study investigating the functional morphological and endocrinological mechanisms behind voice-breaking during the ontogeny of various non-songbirds (Fig. 1B). Natural latex membranes of different length and width could be mounted in an enclosure that simulated the interclavicular air sac (ICAS). This model showed that both the external pressure in the simulated ICAS and membrane dimensions affected the fundamental frequency of the sound, but without a consistent pattern. Both models did not provide any quantification of the membrane properties or vibration. The third mechanical syrinx model was introduced by Brittan-Powell et al. (Brittan-Powell et al., 1997) to study source-tract coupling and consisted of a stretched latex membrane over two holes on opposite surfaces on a 2 mm plastic straw. Membrane vibrations were measured with laser vibrometry in different air densities, and the model demonstrated strong coupling between membrane vibrations and tract resonance properties. For this model, no membrane properties or pressure measurements were performed.

In this paper, we present a mechanical model of the syrinx to study amplitude and frequency control of sound production. We provide a detailed description of the design of our mechanical syrinx model (MSM). Our model allows for detailed quantification of sound production in relation to membrane vibration and mechanical material properties. Furthermore, our model allows for separate control of tension in the vibrating membrane and driving pressure. In this paper we focus on amplitude and frequency control parameters.

MATERIALS AND METHODS

The mechanical syrinx model (MSM)

For a mechanical model approach to study avian phonation, we deliberately stepped back from the biological complexity in terms of morphology and neuromuscular control. We omitted the articulating parts of the upper vocal tract (structures such as larynx, oropharyngeal space, beak), and did not engineer the morphological complexity of the syrinx itself.

During phonation, several forces act on the syringeal labia (songbirds) or membranes (non-songbirds). Firstly the internal syringeal pressure difference between upstream pressure p_u (i.e. bronchial or subsyringeal pressure) and downstream pressure p_d (i.e. tracheal or suprasyringeal pressure; Fig. 1C) causes airflow along the membranes or labia (e.g. Abs, 1980; Brackenbury, 1979; Fee et al., 1998; Gaunt, 1983; Goller and Larsen, 1997a; Goller and Larsen, 1997b; Goller and Suthers, 1996a; Goller and Suthers, 1996b; Laje and Mindlin, 2005b; Nowicki, 1987; Suthers, 1990). Secondly, an external force affects the geometry of and tension in the membranes or labia. This force results from a combination of external air pressure in the interclavicular air sac (ICAS) (e.g. Beckers et al., 2003a; Brackenbury, 1972; Duncker, 1971; Elemans et al., 2008a) and syringeal muscles (e.g. Elemans et al., 2004; Elemans et al., 2006; Elemans et al., 2008b; Gaunt, 1983; Gaunt et al., 1982; Goller and Suthers, 1996a; Goller and Suthers, 1996b). To satisfy the above conditions, we designed a model, which (1) can exhibit self-sustained oscillations and (2) for control of an additional external force that is independent of internal syringeal pressures.

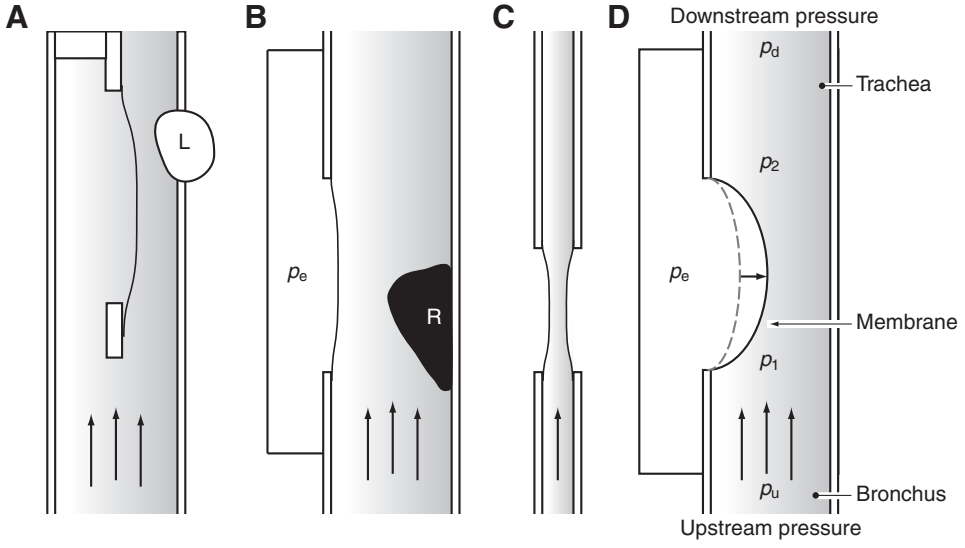

Fig. 1. Schematic representations of mechanical syrinx models. Models by (A) Dürrwang (Dürrwang, 1974), (B) Abs (Abs, 1980), (C) Brittan-Powell et al. (Brittan-Powell et al., 1997) and (D) the model presented here. L, labial imitation; p_d, downstream (tracheal) pressure; p_e, external (air sac) pressure; p_u, upstream (bronchial) pressure; p_1, pressure directly upstream and p_2, pressure directly downstream from membrane; R, dental cement ridge.

Our mechanical syrinx model (MSM) consisted of a 190 mm long aluminium tube (Young's modulus, E=70 GPa) with an inner diameter of 5.6 mm and outer diameter of 8 mm (Fig. 2). An oval hole of 5.5 mm×10.5 mm was milled in the casing of the tube, with the centre of the major axis 97 mm from the distal end of the tube (length L). A latex membrane was mounted over the single hole. We did not design a model with rigid vocal folds (e.g. Deverge et al., 2003; Hofmans et al., 2003), which would not allow the study of amplitude and frequency modulation. Furthermore, in contrast to mathematical models, it is virtually impossible to avoid slight asymmetries [e.g. asymmetries in position, (pre-) tension, density] during the mounting of membranes in a mechanical model. Introducing a morphological symmetry by using two membranes might seem a better representation of the natural situation, but in fact quickly introduces asymmetries in the force balances at play, which consequently leads to a worse representation of the observed behaviour of real folds. Left–right asymmetries are known to lead to additional irregular oscillations in the human vocal folds, such as biphonation (Eysholdt et al., 2003; Mergell et al., 2000; Neubauer et al., 2001). For this reason, mostly only one fold is modelled and symmetry is assumed in mathematical models of sound production in humans [e.g. Ishizaka & Flanagan (1972) and numerous other authors], birds (e.g. Fee et al, 1998; Gardner et al., 2001; Ishizaka & Flanagan, 1972; Laje and Mindlin, 2005b; Laje et al, 2002) and mechanical models of birdsong (Abs, 1980; Dürrwang, 1974). Therefore, in contrast to Brittan-Powel et al, (Brittan-Powel et al., 1997) our mechanical model also contains one membrane instead of two.

We could exert an external force on the membrane because a portion of the tube including the membrane was enclosed in a Perspex (E=3 GPa) cylindrical pressure chamber (internal radius: 33.6 mm, internal length: 54.8 mm) in which we could regulate the pressure independently from the pressure in the tube. This external force mimics the lumped tension exerted by muscles and external loading by a pressure difference with the interclavicular air sac and not the actual pressure in the ICAS. Because this external force is independent of internal syringeal pressures, we were able to uncouple upstream pressure and tension in the membrane. A rectangular window in the pressure chamber allowed observations of membrane movements. All experiments were performed at room temperature in a semi-anechoic room at Wageningen University, The Netherlands.

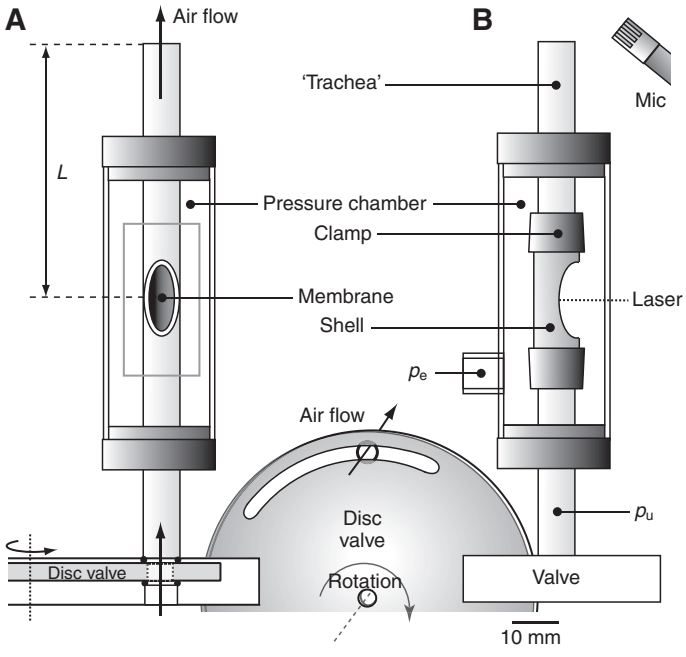

Fig. 2. Schematic representation of the mechanical syrinx model (MSM): (A) frontal and (B) lateral view. In B the clamps and shells for mounting the membrane are shown. The rotating disc valve controls the upstream pressure p_u by closing and opening the tube inlet. The positions of the two pressure transducers (for p_e and p_u) is indicated; L, tube length; mic, location of microphone. Between A and B, part of the rotating valve is show from another view point to reveal its geometry.

Our model design resembles another family of mechanical models named the starling box or starling resistor after its first describer (Knowlton and Starling, 1912). Instead of being a mounted membrane in a rigid tube, the starling box consists of flexible tube that is suspended between two rigid tubes in an external pressure chamber. The starling box setup is used to study fluid flow through collapsible tubes and although the design of our model is different, we will use consistent terminology and symbols with this body of literature (e.g. Bertram, 2004; Bertram and Pedley, 1982; Grotberg and Jensen, 2004).

Experimental setup

The upstream pressure p_u at the inlet of the tube could be controlled with a valve consisting of a motor-driven rotating disc, in which a sickle-shaped slit was milled (Fig. 2). The distance from the valve to the centre of the major axis of the membrane was 93 mm. One rotation of the disc resulted in a periodical pressure pattern. The upstream pressure (p_u) and the external pressure (p_e) were measured with pressure transducers (Statham P23D6, Harvard Apparatus, March-Hugstetten, Germany) at the points indicated in Fig. 2B. The signals from the Statham transducers were amplified (Dual channel amplifier, type EMT 311, Elema-Schönander, Stockholm, Sweden) and low-pass filtered (cut-off frequency 700 Hz). Prior to each measurement the transducers were calibrated with a water column. The pressure amplitudes given in the text are relative to atmospheric pressure, i.e. gauge pressure.

We define the transmural pressure (p_t) as the pressure difference over the membrane:

$$p_t = p_u - p_e \,, \quad (1)$$

where p_u is the upstream pressure and p_e is the external pressure analogous to the collapsible tubes literature (e.g. Bertram, 2004). Note the slight difference in notation and interpretation compared with Elemans et al. (Elemans et al., 2008a), where p_t is defined as the pressure differential between two air sacs as well, but forces exerted by muscles are considered separately.

Membrane velocity was measured with a laser Doppler vibrometer (LDV; controller OFV 3001, sensor head 353, Polytec, Waldbron, Germany). The He-Ne laser beam (wavelength 633 nm) was reflected by a small piece of reflective tape (0.5 mm×0.5 mm) that was glued to the membrane. The inner surface of the aluminium tube was dyed black to prevent reflections from the laser beam. The vibrometer measures the velocity component of the membrane parallel to the laser beam, and the signal was positive if the marker was moving towards the LDV.

Sound was recorded with a 1/4-inch (0.63 cm) omni-directional condenser microphone (type 4939, Brüel and Kjær, Veenendaal, The Netherlands). The microphone signal was pre-amplified (Preamplifier 2670, Brüel and Kjær, Veenendaal, The Netherlands), amplified and band-pass filtered (Nexus Dual channel, conditioning amplifier; high-pass filter 20 Hz, 80 dB dec^{-1}; low-pass 10 kHz,

40 dB dec^{-1}; Brüel and Kjær, Veenendaal, The Netherlands). The front plate of the microphone was placed 3 cm from the tube outlet and directed to the tube outlet from behind, at an angle of 45 deg. with the tube (Fig. 2B) to avoid regions affected by ring vortices coming out of the tube outlet.

Microphone, LDV and pressure transducer signals were digitized at 30 kHz using a 12-bit AD-board (PCI-MIO16E-4, National Instruments, Woerden, The Netherlands) on a Pentium III 700 MHz Workstation. All signal acquisition and analysis software was custom developed in Matlab (The Mathworks, Gouda, The Netherlands).

Digitized signals of the microphone and vibrometer were filtered with a digital band-pass (20 Hz–10 kHz and 20 Hz–5 kHz, respectively) fifth-order Butterworth filter implemented with zero phase-shift ('filtfilt' algorithm in Matlab). Digitized pressure signals from the pressure transducers (p_u and p_e) were filtered with a low-pass (700 Hz) third-order Butterworth filter with a zero phase-shift implementation. The displacement of the laser spot on the membrane was calculated by integrating the velocity signal. This integration introduces a small cumulative error that causes the signal to drift. To eliminate this drift we filtered the displacement signal with a high-pass filter (10 Hz, ninth order Butterworth filter).

Membranes: mounting and material properties

Latex membranes (M1, M2, M3) were made from three different condom types. Condoms provided ideal membrane material, because of the high quality and consistency demands in the intended use. Samples of 40 mm×40 mm were rinsed with water and soap to remove lubricants. The membrane samples were mounted on the MSM by two half-cylinder shells that fitted exactly on the oval hole (Fig. 2B). Pre-load in the samples was kept as close to zero as possible.

Tensile material properties of the membranes were determined using an ergometer (300B, Aurora Scientific, Aurora, Ontario, Canada). To avoid edge effects and ensure mono-axial testing, membrane samples measured 25 mm×1 mm. They were cut either parallel or perpendicular to the base of the condom, to investigate possible anisotropy in the latex. All samples were stored in sealed containers under moist conditions at room temperature. The membrane samples were mounted in the test setup with acrylate glue. With a slider, the length of the samples could be increased by up to 250% of their resting length. Because latex is a rubber composite the elasticity properties are virtually time independent (C. W. J. Oomens, personal communication). Tensile tests were performed with sinusoidal length variations at a frequency of 10 Hz to avoid lateral vibrations in the sample at the minimum longitudinal strain. After testing, the samples were carefully cut out of the set-up and stored at room temperature.

Stress and strain were calculated from the ergometer force and displacement signals, according to Vincent (Vincent, 1982). The nominal stress was defined as $\sigma=F/A_0$, where F is force, and A_0 is the initial cross sectional area. The nominal strain was defined as $\varepsilon=(l-l_0)/l_0$, where l is the actual and l_0 the initial length of the sample. The initial length (l_0) was measured with a digital calliper. We measured cross sectional area (A_0) per sample using a Microphot-FXA microscope (Nikon, Badhoevedorpe, The Netherlands) and Analysis Pro 3.1 software (Olympus, Münster, Germany).

Estimated strain range and mass of the vibrating membrane

Because we only observed sound production when the membrane was either very close to or in full contact with the inner wall of the tube, we could estimate the relevant strain range of the membrane from the two-dimensional tube dimensions (Fig. 3A). In the resting position with both p_u and p_e at atmospheric pressure (p_t=0; see Eqn 1), the length of the membrane l_m was 10.55 mm (line 1 in Fig. 3A). At higher p_t, the membrane is forced into the lumen. When the membrane formed a circular arch with radius 5.2 mm (line 2 in Fig. 3A), it almost touched the opposite side of the tube. The length of the sample was then 16.3 mm (ε=0.55). At even higher p_t, the membrane is pressed against the opposite side of the tube and the membrane deflects sideways (line 3 in Fig. 3A), with l=28.1 mm (ε=1.67). The estimated strain range occurring in the model during the tests was 0.55–1.67 and within this strain range, all tested membranes exhibited linear elastic behaviour.

The mass (m) of the portion of the membrane that is free to vibrate in the mounted situation could not be measured directly. We calculated the maximal free vibrating mass of the membrane from the specific density of the material and the area of the membrane that was enclosed by the clamps. This area was estimated by projecting an ellipse on the cylinders' casing (Fig. 3B). To determine the density per membrane type, four samples of 5 mm×5 mm were cut randomly and weighed (Mettler Toledo AG204, accuracy ±0.1 mg). Their area was measured using a Microphot-FXA microscope (Nikon, Badhoevedorpe, The Netherlands) and Analysis Pro 3.1 software (Olympus, Münster, Germany).

Natural oscillation frequency of the vibrating membrane

Analogous to most musical instruments, we expect that the membranes will vibrate close to their natural frequency (Tack et al., 2006). For a rough approximation, we calculate the natural frequency ω for a two-dimensional clamped, isometric membrane [modified from Fletcher (Fletcher, 1988) after Morse (Morse, 1948)] to be:

$$\omega = C\sqrt{\frac{5T}{\rho \cdot a \cdot H \cdot d}}\,, \qquad (2)$$

where C is a constant (of unity order), T is membrane tension per unit length (N m^{-1}), ρ is the membrane density (kg m^{-3}), a is the tube radius (m), H is the membrane radius (m) and d is the thickness of the membrane (m).

Testing protocols

Mathematical models of the complex fluid–structure interactions during self-sustained oscillations have shown that complex relationships between the tension and/or mass of an oscillating membrane and the frequency can exist (for a review, see Grotberg and Jensen, 2004). However, as a first approximation of the membrane, we use Eqn 2, to formulate several hypotheses: (1) higher tension in the membrane leads to higher frequencies of sound; (2) a heavier membrane (i.e. higher density) leads to lower frequencies of sound; and (3) a stiffer membrane leads to higher frequencies of sound.

Furthermore, if the membrane vibration is coupled to the resonance properties of the distal tube, we expect that a longer distal tube results in a lower fundamental frequency of the sound. To explore the sound production behaviour of MSM, we performed three series of tests, referred to as protocols.

Protocol 1: vibration and sound amplitude

Sound was generated with a simple repetitive p_u pattern supplied by a disc valve with one slit (Fig. 2). Prior to each 'vocalisation' event, p_e was prescribed. The membrane vibrations, pressures and sound were recorded. The signals were binned in segments of 10 ms. Per bin, we calculated the mean p_u, mean p_e, and the root mean square (r.m.s.) value and the spectral density using the multi-taper

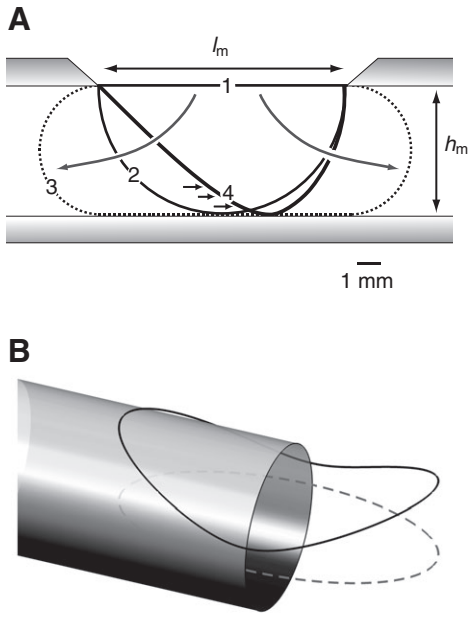

Fig. 3. (A) A medial section through the aluminium tube of the model showing deflections in the membrane with increasing external pressure (p_e). Line 1 represents the membrane at resting length (l_m). With increasing p_e, the membrane deflects more into the tube lumen (curve 2). Curve 3 represents the maximal length of the membrane during experiments. When air is flowing trough the tube (from left to right) the membrane deforms (curve 4). l_m=10.55 mm; h_m=5.6 mm. (B) To estimate the area of the vibrating membrane, an ellipse is projected on the tubes' casing.

method (Percival and Walden, 1993; Thompson, 1982) of sound and vibrometer signals. Segments were zero-padded to 8096 points to obtain a frequency resolution of 3.7 Hz.

Protocol 2: frequency control space

To explore the behaviour of the model as a function of the p_u–p_e pressure parameter space, we systematically altered pressures p_u and p_e. First, both pressures were set to atmospheric pressure. Second, a certain value of p_e was set and p_u was increased in discrete steps. This procedure was repeated for increasing values of p_e. The produced sound, p_e and p_u were recorded for 1 s. The highest value of p_e was qualitatively judged based on experience of previous rupture events. For every recording, we determined the mean value of p_e ($\bar{p}_e$) and p_u ($\bar{p}_u$) and the spectrum of the sound to calculate the fundamental frequency (f_0) and the harmonics ratio (see Eqn 4). Mean values of fundamental frequency data were fitted on a 2-D mesh of $\bar{p}_e$ and $\bar{p}_u$ with a grid spacing of 200 Pa. We omitted recordings with sound pressure level, SPL [SPL=20log(p/p_0) with reference pressure p_0 of 20 μPa] lower than the background noise level of 50 dB SPL and with f_0 lower than 400 Hz. The latter were generally recordings of membrane flutter or eolic (i.e. turbulent) noise. To investigate the effect of membrane properties on the behaviour of the model, we repeated this protocol with three types of membranes with different material properties.

Membrane tension

Because the transmural pressure applies a force on the membrane, we expect that membrane tension, K, changes with the transmural pressure: $K \propto p_t = p_u - p_e$. In our model, a certain constant amount of external pressure p_e is needed to displace the membrane so it touches the inner side of the tube (lines 2–4 in Fig. 3), before an increase in upstream pressure p_u can cause self-sustained oscillations of the membrane. In the static situation with p_u=0, this initial external pressure (p_{e0}) is defined by the elastic properties of the membrane. Because we were interested in the tension increase of the membrane during sound production, we needed to offset our tension parameter for this initial external pressure:

$$K \propto p_u - (p_e - p_{e0}) . \quad (3)$$

We estimated p_{e0} per membrane type by extrapolating the lower bound p_u values associated with self-sustained oscillations to p_u=0.

Intensity decay of harmonics

The sound produced by the model is rich in harmonics. To study the spectral shape of the produced harmonics, we define a simple measure – the harmonics ratio (HR):

$$\mathrm{HR} = -\frac{1}{n}\sum_{i=1}^{n} 10\log_{10}\left(\frac{H_0 - H_n}{i}\right), \quad (4)$$

where H_n is spectral amplitude (in Pa Hz^{-1}) of the n^{th} harmonic and H_0 is the fundamental (Zaccarelli et al., 2006). We calculated HR for the range i=3–8. This quantity is closely related to the spectral slope (e.g. Titze, 2002; Sciamarella and D'Alessandro, 2004). For example, with i ranging from 3 to 8, an HR of –5 dB indicates an average decrease of 5 dB per harmonic over the 3rd to 8th harmonic.

Protocol 3: source-tract coupling

To investigate the coupling between sound production and distal tube length, the length, L, of the tube (Fig. 2A) was increased systematically. Tube extensions of 2, 4, 6, 8, 10, 15, 20, 30, 40, 50, 60, 80 and 90 cm were attached to the tube outlet of the MSM mounted with membrane M2. First, pressures p_e and p_u were prescribed to generate sound. Subsequently, extensions of increasing length were placed on the tube outlet. Upstream pressure and sound were recorded for 1 s to calculate the mean p_e, p_u and fundamental frequency of the sound. The resonance frequency for a tube open at both ends is:

$$H_k = kc/2L (k = 1,2,3,...,N) \quad (5)$$

and for a tube closed at one end is:

$$H_k = kc/4L (k = 1,3,5,...,N) , \quad (6)$$

where H_k is the resonance frequency of the k^{th} mode, c is the sound speed (344 m s^{-1} at 20°C and sea level), and L is the tube length.

RESULTS

Protocol 1: vibration and sound amplitude

Fig. 4 shows traces of sound pressure, membrane velocity and upstream pressure during two rotations of the disc valve. Raising the upstream pressure (p_u) above a threshold value results in high frequency (>600 Hz) self-sustained oscillations of the membranes. We only observe sound production when the pressure in the air sac p_e is set to an initial value sufficiently high to result in complete closure of the tube by the membrane at p_u=0. Modulating p_u results in modulation of the amplitude of membrane velocity and sound pressure (Figs 4 and 5). The first peak in p_u at the start of every 'syllable' (arrow in Fig. 4C) is caused by the pressure head that emerges when the rotating disc valve opens. Spectrograms of sound and vibration signals show a harmonic stack with even and odd harmonics (Fig. 4D,E).

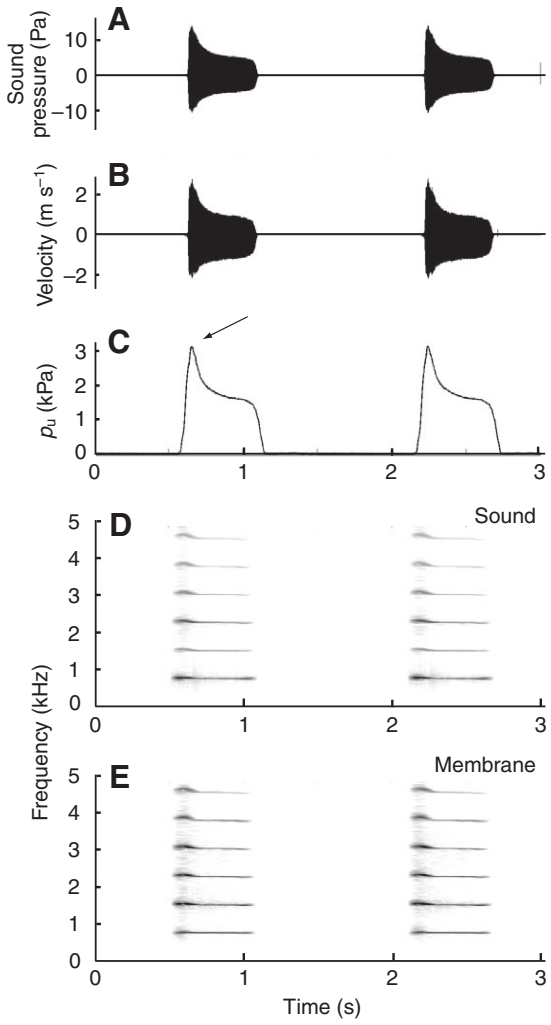

Fig. 4. Typical results from a time series of (A) sound pressure; (B) membrane velocity, and (C) upstream pressure, p_u. The arrow indicates the pressure head that emerges from the disc valve. Rotation frequency of airflow valve=1.6 Hz. Mean p_e=5.58 kPa. (D) Spectrogram of sound and (E) of membrane velocity.

The relationship between sound amplitude and membrane velocity as a function of upstream pressure of four consecutive 'syllables' is linear over most of the range (Fig. 5). Above a threshold value of p_u, the 'onset threshold', the membrane behaviour bifurcates from static to self-sustained oscillation and sound is produced. The membrane remains in the oscillatory state until pressure decreases from 3 to 1.5 kPa below the onset threshold, the 'offset threshold'. The hysteresis effect associated with higher phonation onset pressure and lower phonation offset pressure has been well documented (Lucero, 1999). The onset pressures decrease slightly between consecutive 'syllables' during the recording shown in Fig. 5. This can be caused by small fluctuations in the external pressure in the pressure chamber (p_e), slight material relaxation or even slight heating, which would lower the stiffness.

The sound intensity is very high; the sound pressure level increases up to 10 Pa in the recording shown in Fig. 4A, which corresponds to a sound intensity of 114 dB (re. 20 μPa). This is because the microphone is placed in the acoustic extreme near-field and as such picks up both pressure and particle movement. The membrane velocity shows a similar relation with p_u as sound amplitude (Fig. 5C). With increasing upstream pressure, the fundamental frequency of the produced sound and of the membrane velocity increases linearly from 750 to 800 Hz (Fig. 5B,D). For both amplitude and frequency, the relationship with p_u deviates slightly from a linear relationship close to the phonation offset (p_u<1.4 kPa). The valve is closing at this point during the rotation cycle of the valve, which alters the flow–pressure relationship.

Sound production is tightly associated with membrane vibration: a close relationship exists between the amplitude patterns of sound and membrane vibration (Fig. 5A,C). This close relationship also exists in the spectral domain: Fig. 6 shows the very strong relationship between the fundamental frequency of the membrane velocity and the fundamental frequency of the sound pressure (linear regression; R^2=0.97, P≪0.001, N=2672).

Fig. 7 shows an example of a typical onset of sound (Fig. 7A) and membrane displacement (Fig. 7B). The maximal measured displacement of the membrane is 0.25 mm. The membrane deflections during phonation are small (<5%) compared with the inner diameter of the tube (5.60 mm). The spectral density estimates of sound and membrane velocity show that these signals are rich in both odd and even harmonics of the fundamental frequency (Fig. 7C,D). To check whether the model wall was resonating because of the produced sound, the vibrations of several parts of the model were measured during sound production. At all investigated points on the tube and the pressure chamber, vibrations were below noise level of the LDV and could not be extracted even after averaging.

Protocol 2: frequency control space

We tested three membranes (M1, M2, M3) that all exhibited linear elastic behaviour in the strain range occurring during phonation events (Fig. 8, linear regression: M1: R^2=0.999, P≪0.001; M2: R^2=0.995, P≪0.001; M3: R^2=0.995, P≪0.001). Table 1 contains the measured and estimated membrane material properties.

We investigated the dynamic oscillation behaviour of the membranes in the p_u, and p_e control space. Fig. 9A–C shows that both abrupt transitions between oscillatory modes as well as gradual modulation of sound fundamental frequency occur depending on both p_u and p_e for all membranes. In the upper left corner of the control space, p_e is high enough to close off the tube completely; no sound is produced. In the bottom right corner, high values of p_u impose risk of rupture of the membranes. Not every combination of p_u and p_e can be realised experimentally; at a low p_e it is not possible to get a high p_u since the air resistance in the tube is low, and at high p_u and p_e, the membrane ruptures.

Fig. 9A–C also shows that the phonation onset pressure for every membrane increases with increasing external pressure (p_e): as p_e is set to a higher value during the protocol, the minimal p_u required to push away the membrane and induce self-sustained oscillation increases. The initial external pressure (p_{e0}, see Eqn 3) is constant per membrane type and measured 7.4, 4.7 and 6.4 kPa for M1, M2 and M3, respectively, at p_u=0 (red p_t isolines in Fig. 9A–C). It should be noted that when p_e equals p_{e0}, p_u is zero. Therefore the membrane is not excited by flow, and no vibration occurs.

Fig. 9D–F show the fundamental frequency (f_0) as a function of tension parameter K (Eqn 3) and upstream pressure p_u for the three membranes. For all three membranes, the f_0 increases with increasing tension K and also with upstream pressure p_u. The three membranes occupy different ranges in the control-space for both pressures and produced fundamental frequencies. The frequency ranges of the oscillations for the three membranes are 812–900 Hz, 629–930 Hz and 751–872 Hz for M1, M2 and M3, respectively. It should be noted that the upper frequency boundary is based on the subjective

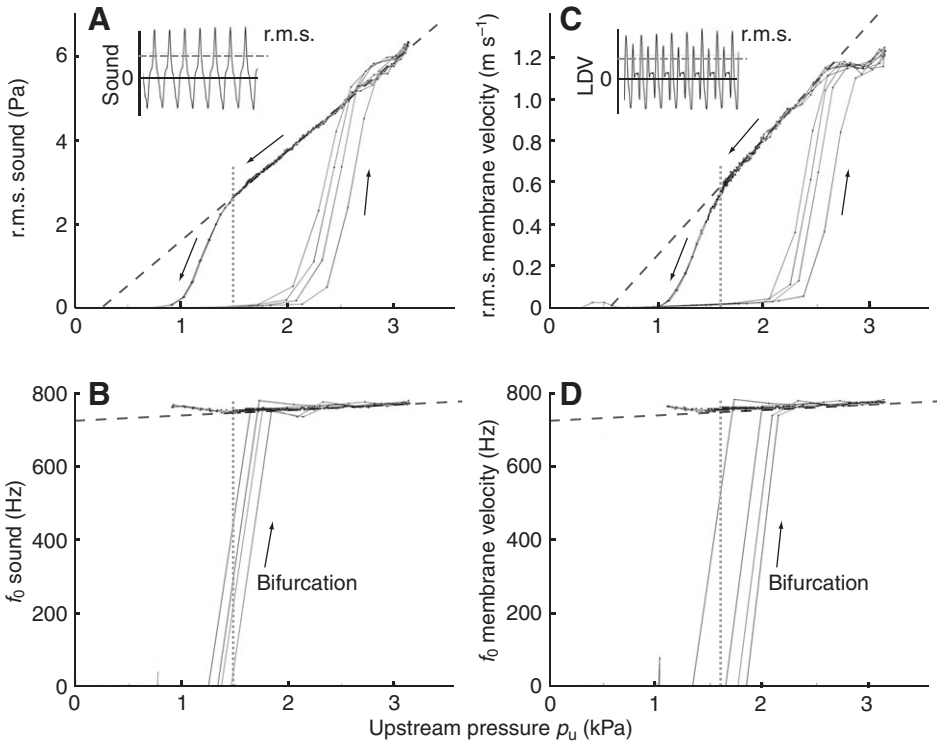

Fig. 5. Sound and membrane parameters as a function of upstream pressure. (A,C) Root mean squares (r.m.s.) of sound pressure values of (A) sound pressure and (C) membrane velocity. The arrows indicate the progression of time. The insets show a single exemplary bin of the recorded signals with r.m.s. values. (B,D) Fundamental frequency of (B) sound and (D) membrane velocity. The behaviour of the membrane changes instantly from no movement to oscillation at about 750 Hz, which represents a bifurcation of this nonlinear system.

risk of membrane rupture and as such does not provide much information. We do not observe any trend between Young's modulus and the lower bound fundamental frequency (Fig. 10A), but we observe the trend that a heavier membrane increases the lower bound fundamental frequency (Fig. 10B).

The amount of harmonic decay changes with p_u and tension K, but not consistently with either one parameter. The membranes exhibit modulation of the harmonics ratio HR (Eqn 4) in a range from –9.7 to 1.8, with a tendency towards higher values at higher p_u, which means that at higher upstream pressure the higher harmonic decay is less and consequently the harmonics get stronger, which is consistent with observations by Abs (Abs, 1980). However no consistent pattern was observed.

Protocol 3: source-tract coupling

To investigate the coupling between produced sound and tube resonances, we systematically altered the length of the tube downstream to the membrane of the MSM. The fundamental frequency f_0 closely follows the first resonance frequency (H_1) of a tube closed at one end (Fig. 11A). However, a difference between the measured f_0 and predicted H_1 of the tube exists and it decreases with increasing tube length. This discrepancy between observed and predicted values can be explained if we consider the column of oscillating air in the tube distal to the membrane. When at resonance, the air column moves back and forth in the tube and a small volume of air moves in and out of the tube at the tube outlet. In a tube open on one end, this air volume is only dependent of the tube diameter and increases the 'effective length' of the resonating air column (e.g. Kinsler et al., 1982). In our model, we can expect that both the open end of the tube as well as the membrane affect the effective length of the tube. To obtain the effective length of the air column, we need to add a so-called 'end correction' to the measured tube length. We consider only the first resonance and modify Eqn 6 into:

$$H_1 = v/4\,(L + \Delta)\,, \qquad (7)$$

where L is the tube length and Δ is the end-correction. For convenience, we can rewrite this equation as

$$L + \Delta = \left(\frac{v}{4}\right)\frac{1}{H_1}\,. \qquad (8)$$

By plotting measured tube length versus 1/H1, we can read Δ directly from the plot (Fig. 11B, linear regression, R^2=0.999, $P \ll 0.001$). In Fig. 11B the slope is equal to the speed of sound divided by four, and where y=0, the x-value equals the negative end correction Δ. The end correction for our syrinx model with the used membrane measures 13.4 mm. From this protocol, we can conclude that the

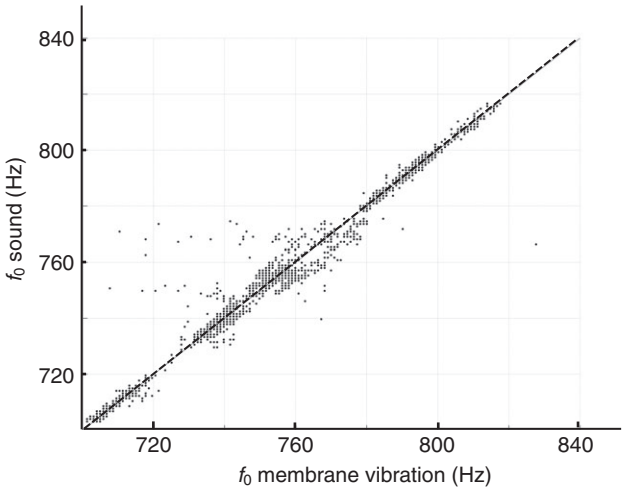

Fig. 6. Fundamental frequency of the vibrating membrane correlates tightly with the fundamental frequency of the produced sound (linear regression; R^2=0.97, $P \ll 0.001$, N=2672).

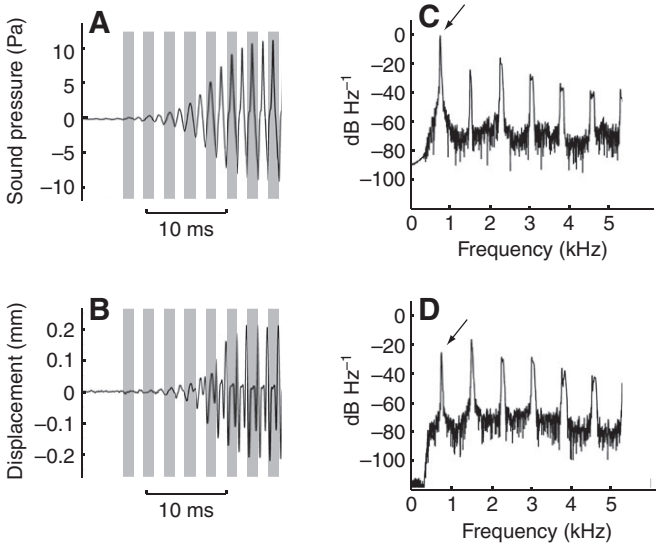

Fig. 7. (A,B) Detail of (A) sound wave and (B) membrane displacement. Single oscillation periods of the sound pressure (grey bars) correspond to periods of the membrane position. (C,D) Spectrum estimates of the signals shown in A and B, respectively. Arrows indicate the fundamental frequency.

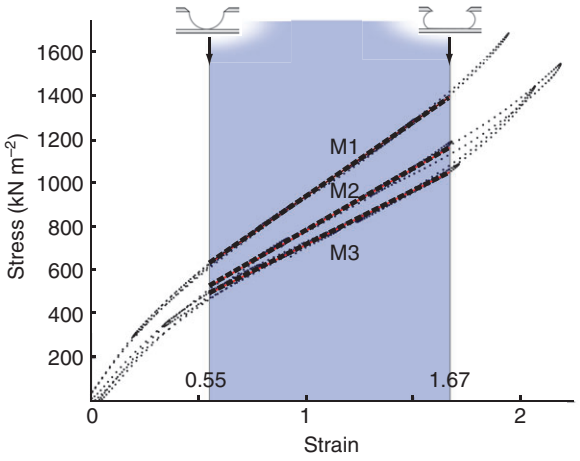

Fig. 8. Dynamic tensile tests of the membranes M1, M2 and M3. Thick dotted lines show the results of linear regression per membrane. The blue shaded area indicates the estimated strain range (0.55–1.67) that occurs during phonation, according to Fig. 3.

oscillation frequency of the membrane is strongly coupled to the first resonance frequency of the tube.

DISCUSSION

We present a mechanical syrinx model (MSM) that allows for detailed measurement of membrane vibration and sound production. We show that increasing membrane tension K leads to higher fundamental frequency (f_0), which is a common assumption underlying mathematical models of birdsong (e.g. Elemans et al., 2008a; Gardner et al., 2001; Laje and Mindlin, 2002; Laje et al., 2002; Mindlin et al., 2003). Some mathematical models also assume a separate uncoupled control of labial or membrane tension and driving pressure by syringeal and respiratory muscles, respectively (Gardner et al., 2001; Laje and Mindlin, 2002; Laje et al., 2002; Mindlin et al., 2003). This enables birds to generate a wide variety of song syllables with just simple sinusoidal variations of the control parameters in their parameter space (Gardner et al., 2001) using simple neural instructions (Laje and Mindlin, 2002). Because we can control pressure p_u and tension K separately in the MSM, we can construct a wide variety of 'syllables' with simple sweeps of the control parameters (ellipses in Fig. 9e), where the time course of tension K and pressure p_u traces out the time course of the fundamental frequency (Fig. 9) and the amplitude (Fig. 5) of the 'syllable', respectively, analogous to 'syllables' presented in simplified mathematical models of avian song (e.g. Gardner et al., 2001; Laje and Mindlin, 2005a; Laje and Mindlin, 2005b; Mindlin et al., 2003).

We show that in our model both the amplitude and fundamental frequency (f_0) of membrane self-sustained vibrations correlate tightly with the amplitude and f_0 of the radiated sound (Figs 4, 5 and 6). The oscillating membrane surface modulates the downstream airflow: a single oscillation cycle of the membrane is associated with a single oscillation of the recorded sound wave (Fig. 7) and the fundamental frequency of the membrane oscillation and sound are highly correlated (Fig. 6). Membrane oscillations can become self-sustained when Bernoulli forces counteract elastic forces, which require the membrane to be in close proximity with the other wall. Therefore the external pressure is high when the membrane bulges inwards far enough to allow oscillations. Because sound can be generated at much smaller differences between air sac and bronchial pressure in *in vivo* (e.g. Brackenbury, 1972) and in *in vitro* preparations (Abs, 1980; Dürrwang, 1974; Fee et al., 1998; Paulsen, 1967; Rüppel, 1933), our model differs from the natural situation. Other mechanical models successfully achieved flow-induced vibrations of a membrane at lower external pressures by inserting an additional structure, a lump of dental cement in Abs (Abs, 1980) and an unspecified 'labial imitation' in Dürrwang (Dürrwang, 1974), or by having an entire flexible wall (e.g. Luo and Pedley, 1996).

The oscillating structures in the syrinx are often referred to as the sound sources or sound producers, which is an oversimplification of the phenomena at play. Several physical mechanisms of sound production exist when flow induces the vibration of a membrane: the vibration of the membrane itself (a vibrating membrane without mean flow could still radiate sound), the pulsatile airflow passing

Table I. Measured and calculated membrane properties

Type	Membrane density ρ_s (g m^{-2}; N=4)	Membrane mass m (mg)	Young modulus E (kPa)	Natural frequency ω_n (Hz)
M1	104±5.0	2.70±0.13	957	35
M2	63.2±2.0	1.63±0.05	874	42
M3	92.9±4.0	2.40±0.10	774	33

The natural frequency, ω, was calculated according to Tack et al. (Tack et al., 2006). We assumed a thickness, length and width to be 0.1 mm, 10.5 mm and 5.0 mm, respectively.

the valve (i.e. model membrane or syrinx) causing a fluctuating pressure within the tube, the interaction (e.g. impinging, shearing) of the airflow with structures (e.g. the membrane and tube walls), and turbulent air fluctuations. All of these sound sources are present at different relative levels of magnitude and can even fluctuate over the period of one oscillation (see e.g. Zhao et al., 2002). Because the MSM never produced sound without the membrane touching the opposite wall, the fluctuating pressure within the tube caused by the pulsatile airflow when the membrane opens and closes is perhaps the most dominant sound-producing mechanism, but it is not possible to be conclusive.

Mechanics of sound production

The behaviour of the system bifurcates from a stable to an oscillating membrane as the parameter values are varied, especially in a narrow region near the positive diagonal of the p_u, p_e-control-space (Fig. 9A–C), which means that the critical values of p_e themselves depend on p_u (Bertram, 2004). This phenomenon has been identified in the collapsible tube literature (e.g. Bertram et al., 2004; Grotberg and Jensen, 2004; Pedley and Luo, 1998) and to increase the resolution in this area, instead of p_e, the pressure difference p_e–p_2 (=p_{e2}) is often used as a modified control parameter, where p_2 is the pressure directly downstream of the membrane (see Fig. 1C) (e.g. Brecher et al., 1952; Bertram, 1986; Bertram et al., 1990; Bertram et al., 1991; Conrad, 1969). In contrast to the classic starling box, our model's downstream outflow is into an open room, and p_d equals atmospheric pressure. However, we cannot reliably derive p_2 from the pressure drop p_1–p_d (see Fig. 1C) and therefore we did not correct our p_u, p_e-control space to a modified p_u, p_{e2}-control space. Nevertheless, the p_u, p_e-parameter space obviously controls the oscillatory state of membrane and modulates the fundamental frequency of the oscillation.

As mentioned above, our model resembles the classic starling box used in collapsible tube studies. Many mathematical models

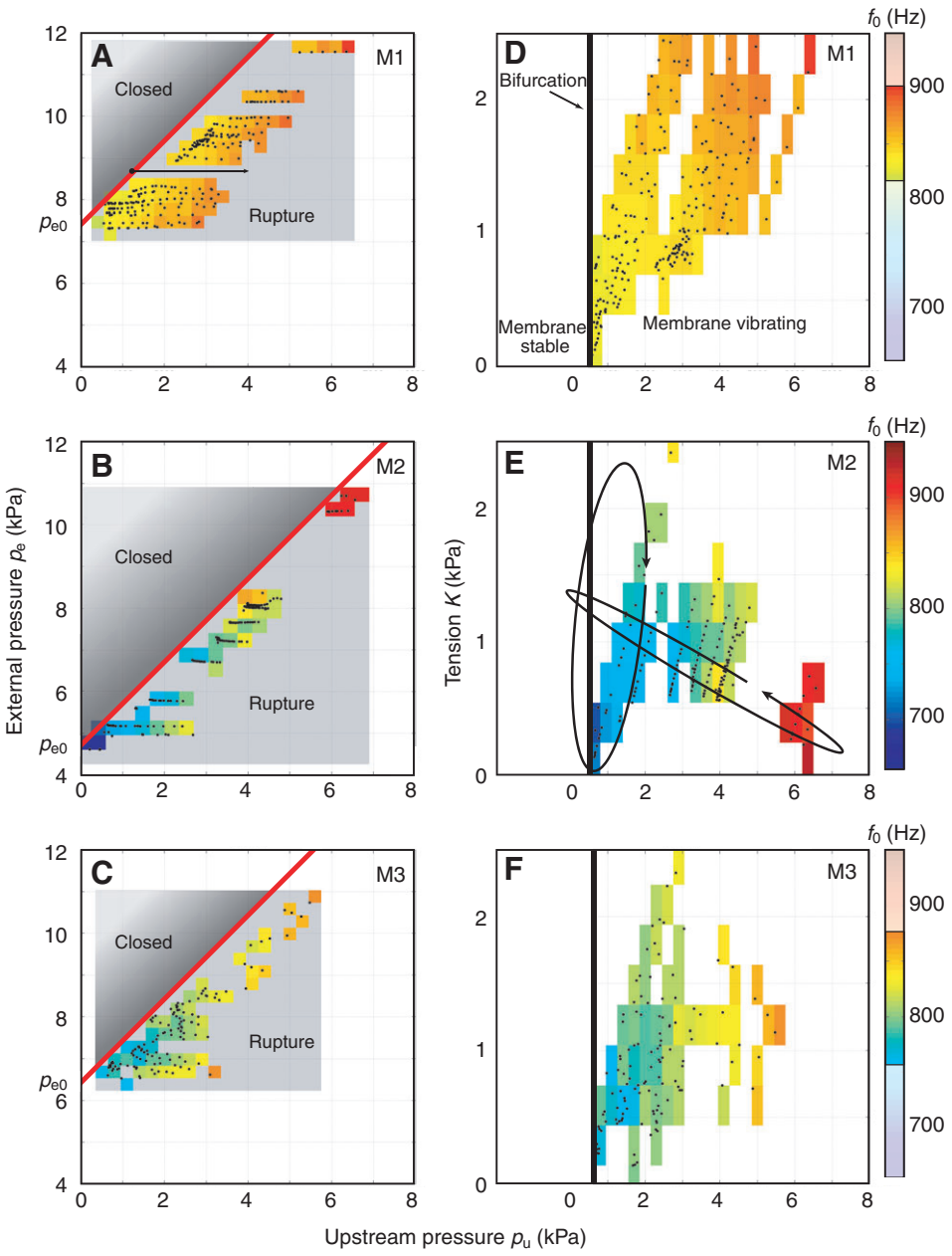

Fig. 9. (A–C) Fundamental frequency in the upstream and external pressure control space for the three different membranes M1 (A), M2 (B) and M3 (C). Dots indicate the exact measurement locations. The colours show mean fundamental frequency f_0 of the measurements in the specific grid cell. The bright coloured section of the colour bar shows the range of f_0 measurements. Red isolines indicate the minimal transmural pressure needed for sound production. (D–F) Fundamental frequency in the tension K and upstream pressure p_u control space for the three different membranes The elliptical arrows in E indicate possible paths to create the sound syllables (see Discussion).

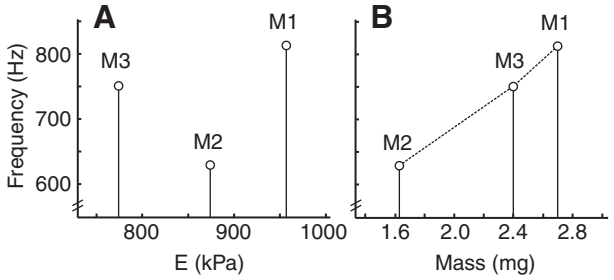

Fig. 10. Lower bound of fundamental frequency range as a function of (A) Young's modulus and (B) mass (Table 1) for membranes M1–3.

have been developed to study the complex fluid-membrane interactions in collapsible tubes for various conditions [e.g. low and high Reynolds numbers (see Bertram and Castles, 1999; Hazel and Heil, 2003; Heil, 1997; Jensen and Heil, 2003; Lyon et al., 1981) and three-dimensional membrane fluid interactions (see Hazel and Heil, 2003; Marzo et al., 2005; Thompson et al., 2004; de Vries et al., 2002; de Vries et al., 2003)]. Nevertheless, the actual mechanisms that control the self-sustained oscillations are still under debate. Here, our focus is on high-frequency self-excited oscillations and not on pressure–flow relations in other parts of the parameter space. Several studies report high-frequency oscillation (e.g. Jensen and Heil, 2003). Bertram and colleagues studied the highest frequency oscillations in this context and they report complex waveforms up to 100 Hz (e.g. Bertram and Castles, 1999; Bertram et al., 1991). Our model operates in a different parameter range, at higher frequencies of self-sustained oscillation and with a higher tension in the membrane.

Besides the bifurcation behaviour of the system from a stable to oscillating membrane, we also observed some other signatures of nonlinear behaviour in our model. When pressure was increased (obviously also leading to very high flow rates), abrupt jumps to noisy sounds were observed. Rich nonlinear behaviour is also commonly observed in *in vitro* studies of birds (Fee et al., 1998), excised larynges of dogs (Berry et al., 1996), frogs (Suthers et al., 2006) collapsible tubes (Bertram et al., 1991; Armitstead et al., 1996) and, although not recognised as such, in a previous syrinx model (Abs, 1980). The combination of self-sustained oscillations with a forced pressure oscillation, such as an oscillating driving pressure by respiratory muscles, can cause very rich dynamic vibratory behaviour of the membrane (She and Bertram, 1996). Because this combination is a common physiological phenomenon in birdsong, it could be an important source of nonlinearities that has received virtually no attention so far.

Range of produced frequencies

We show that the lower bound frequency of the full frequency range increases with mass of the membrane used (Fig. 10B), which is consistent with the findings of Abs (Abs, 1980). However, it is the opposite of what we would expect if we use a definition of fundamental frequency derived from models based on simple string (Tack et al., 2006) or two-dimensional membrane models [Eqn 2; cf. Fletcher (Fletcher, 1988)]. Although this might be unfortunate for the sake of simplicity, it is not necessarily surprising; these models are approximations when the deflections are small and close to the resting positions of the membrane. Although the oscillation amplitude of the membrane in our model is small compared with the tube diameter, the oscillations do not occur around the resting position of the membrane, but under high strains.

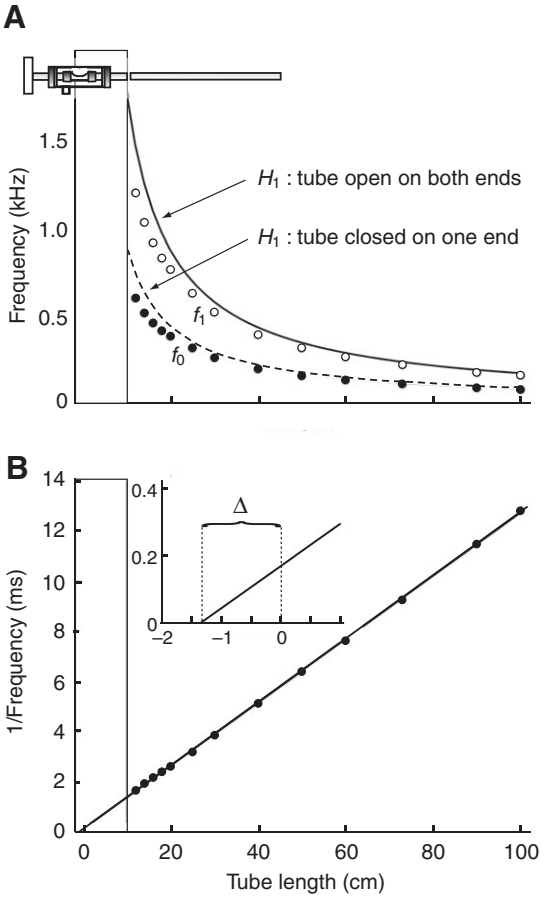

Fig. 11. The effect of distal tube elongation on the frequency of the produced sound. (A) Tube length *versus* the measured fundamental (f_0: closed circles) and first harmonic (f_1: open circles). The two lines show the lowest resonance frequency (H_1) of a cylinder that is, respectively, open (solid line: Eqn 5) or closed on one end (dotted line: Eqn 6). (B) Regression of the measured fundamental frequency (closed circles) to estimate the end correction Δ (see Results). R^2=0.997, P<0.01.

In the MSM, the membrane is not vibrating freely, because: (1) the calculated natural frequencies of the different membranes are 20- to 30-fold lower than the self-sustained oscillation frequencies observed during the various protocols (compare 30–40 Hz in Table 1 with 600–900 Hz in Fig. 9) and (2) we observe that the oscillations are strongly coupled to the resonance frequencies of the distal tube length (Fig. 11).

Source-tract coupling

Sound production in our model is strongly coupled to the tract resonances, as can be seen in Fig. 11. To obtain the effective length of the resonating air column, we corrected the measured tube length with the length or end correction Δ. This end correction was 13.4 mm in our model and accounts for the small volume of air that moves in and out of the tube at the membrane and at the tube outlet. Therefore, the end correction Δ equals the addition of the 'classic' end correction at the tube end Δ_{end}, and the end correction at the side of the vibrating membrane Δ_{mem}. The theoretically predicted end-correction Δ_{end} of an open unflanged pipe is 0.6 times the radius of the pipe (Kinsler et al., 1982), which, in the case of our model, would correspond to 0.6×3 mm=1.8 mm. The end correction at the membrane Δ_{mem} equals 11.6 mm.

The length of the distal tube L was measured from the centre of the membrane (Fig. 2) and the length of the membrane l_m was 10.55 mm (Fig. 3A). From our calculated end correction, we can conclude that from this point an additional 11.6 mm of upstream tube affects the resonating air column in the distal tube. Beside the mass of the air in the column, the mass of the membrane also probably adds to the effective length of the distal tube.

As also observed by Fitch (Fitch, 1999), there seems to be a difference in behaviour between the *in vivo* and *in vitro* syringeal system. *In vitro* studies with excised syringes demonstrate strong coupling (Rüppel, 1933) [but see Miller (Miller, 1934)], whereas weak coupling is mostly observed in the *in vivo* system (Nowicki, 1987). The mechanical models of Abs (Abs, 1980) and Dürrwang do not exhibit strong source-tract coupling (unfortunately no details on the setup downstream are given), and the mechanical models consisting of straws by Brittan-Powell et al. (Brittan-Powell et al., 1997) exhibited strong coupling. A possible reason for the strong coupling might be found in the material properties of the distal tube. The stiff aluminium walls used in our model are strongly reflective for pressure waves and might therefore decrease the amount of energy lost to wall absorption. The consequent increase in energy in the tube could increase the coupling of source and resonator. This hypothesis could explain the stronger coupling observed in *in vitro* preparations. Because smooth muscle tissue in the tracheal lining and tracheal striated muscles go into a state of rigor when dead, the vocal tract is expected to be much stiffer compared to *in vivo*. It is unknown what happens to the stiffness of syringeal muscles after nerve cuts (Brittan-Powell et al., 1997).

Another explanation of the presence of strong coupling in our model may be found in the difference between the resonance frequency of the oscillating membranes and the tube. Fletcher (Fletcher, 1988) suggested that the oscillation frequency of the syrinx is determined by one or two dominant resonant modes of the oscillating structures. This has been confirmed in excised syrinxes of the zebra finch (*Taenopygia guttata*), in which the medial vibratory masses (MVM, i.e. medial labium and medial tympaniform membrane) have a strong vibrational mode around 600 Hz (Fee, 2002), which closely resembles the fundamental frequency of the lower syllables of normal song. Also in humans, the vocal folds oscillate close to dominant resonance frequencies (e.g. Švec et al., 2000). In our model, however, the membrane has a 10-fold lower resonance frequency than the tube, which might have enforced the coupling between membrane oscillation and upstream geometry.

Despite the strong coupling, we still observe that the fundamental frequency is modulated with tension caused by the applied external force. A small part of this frequency range can be explained by the shifting position and geometry of the membrane. As a result of the aerodynamic forces on the membrane when upstream pressure increases, the geometry of the membrane may change from line 3 to line 4 (Fig. 3A). This change in geometry may change the effective length of the resonating air column and therefore the fundamental frequency of the radiated sound. If we assume that the point where the membrane touches the opposite wall can maximally shift from 97 towards 92 mm from the tube end, this will cause an increase in resonance frequency from 780 to 820 Hz. The shifting position and geometry can account only for a small part of the observed frequency modulation range.

In birds, additional mechanisms may be used to modulate frequency, but the extent to which this occurs or is employed by different species is unknown. For example, in addition to tension, any mechanism that affects the redistribution of effective vibrating mass (the product of the parameters density and dimension in Eqn 2) will affect the oscillation frequency (c.f. Fee, 2002; Fletcher, 1988). Because selective damping of the medial labia in zebra finches results in an increase in its resonance frequency (Fee, 2002), it may be possible that birds use this mechanism during sound production. Furthermore, Fee (Fee, 2002) speculates that by positioning their lateral labium close to the opposite medial labium, zebra finches might be able to restrict the spatial extent of resonant modes of the MVM, like placing a finger on a guitar string. This would also increase the dominant resonant mode of the MVM (medial labium and membrane).

The upper vocal tract is important for sound production (Beckers et al., 2003b; Beckers et al., 2004; Daley and Goller, 2004; Goller et al., 2004; Nowicki, 1987) and sound radiation efficiency: the opening of the larynx enhances radiation of sound in ring doves (Fletcher et al., 2005) and the shape of the oropharyngeal space in cardinals enhances radiation of the fundamental frequency (Fletcher et al., 2006; Riede et al., 2006). From modelling studies, we know that acoustic feedback of the tract can even alter source vibrations (Hatzikirou et al., 2006; Laje et al., 2001; Laje and Mindlin; 2005a). We observed occasionally that partial flaring of the distal tube in the MSM resulted in stable oscillations at higher frequencies and we speculate that controlling jumps to other stable modes of oscillation could be an additional function of the avian larynx.

Syringeal morphologies

The elastic membrane used in our study is an attempt at a better approximation to real avian anatomy. In addition to membrane dimensions (Abs, 1980), we show that material properties also alter the frequency range of sound production. The membranes used in the model consist of isotropic latex and their structure is more consistent than natural rubber (Abs, 1980) and far less complex than that of the real oscillating structures. The histological ultrastructure of labia in oscines has received virtually no attention and only a few studies exist on the histological ultrastructure of the lateral and medial tympaniform membranes of non-oscines. The lateral tympaniform membranes in the mallard (*Anas platyrhynchos*) and Japanese quail (*Coturnix japonica*) are regionally differentiated structures with different layers of epithelium and fibres (Bayram and Liman, 2000; Frank et al., 2006; Scala et al., 1990). Therefore, the mechanical behaviour of labia or syringeal membranes is likely to be anisotropic, i.e. different in mechanical properties with orientation and dynamics of the applied load (e.g. Fee, 2002).

Our mechanical model confirms some of the basic assumptions underlying models for sound production in birds. An amazing variety of different syringeal morphologies have evolved within birds to produce vocalisations (King, 1989). It is therefore unlikely that all species employ the same mechanisms to make and control their vocalisations. By simplifying the avian vocal system to a simple nonlinear oscillator, the complex geometry and distribution of material properties are necessarily sacrificed for the focus on neural control. To understand these complex and different morphological designs from a biomechanical and evolutionary point of view, we need to include more realistic geometries in future syrinx models.

LIST OF ABBREVIATIONS

EMG	electromyography
HR	harmonics ratio
ICAS	interclavicular air sac

K	tension in membrane
MSM	mechanical syrinx model
p_d	downstream pressure (i.e. tracheal or suprasyringeal pressure)
p_e	external pressure
p_t	transmural pressure
p_u	upstream pressure (i.e. bronchial or subsyringeal pressure)

The investigations were (in part) supported by the Research council for Earth and Life Sciences (ALW) with financial aid from the Netherlands Organisation for Scientific Research (NWO). The authors wish to thank E. Jansen, E. Karuppannan, M. Schimmel and J. Theunissen (Mechanical Workshop/Wageningen University) for constructing and contributing to the development of our mechanical model, condomshop 'Het Gulden Vlies' (Amsterdam) for making the model whistle, C. W. J. Oomens for advise on the tensile tests and C. Bertram, M. Hirschberg, X. Pelorson for advise and discussion, and two anonymous referees for helpful and constructive comments on the manuscript.

REFERENCES

Abs, M. (1980). Zur Bioakustik des Stimmbruchs bei Vögeln. *Zool. Jb. Physiol.* **84**, 298-382.
Armitstead, J. P., Bertram, C. D. and Jensen, O. E. (1996). A study of the bifurcation behaviour of a model of flow through a collapsible tube. *Bull. Math. Biol.* **58**, 611-641.
Bayram, G. and Liman, N. (2000). A morphological investigation of the postnatal development of the syrinx in the quail. *Turk. J. Vet. Anat. Sci.* **24**, 381-392.
Beckers, G. J. L., Suthers, R. A. and ten Cate, C. (2003a). Mechanisms of frequency and amplitude modulation in ring dove song. *J. Exp. Biol.* **206**, 1833-1843.
Beckers, G. J. L., Suthers, R. A. and ten Cate, C. (2003b). Pure-tone birdsong by resonance filtering of harmonic overtones. *Proc. Natl. Acad. Sci. USA* **100**, 7372-7376.
Beckers, G. J. L., Nelson, B. and Suthers, R. A. (2004). Vocal tract filtering by lingual articulation in a parrot. *Curr. Biol.* **14**, 1592-1597.
Berry, D. A., Herzel, H., Titze, I. and Story, B. (1996). Bifurcations in excised larynx experiment. *J. Voice* **10**, 129-138.
Bertram, C. D. (1986). Unstable equilibrium behaviour in collapsible tubes. *J. Biomech.* **19**, 61-69.
Bertram, C. D. (2004). Flow phenomena in floppy tubes. *Contemp. Phys.* **45**, 45-60.
Bertram, C. D. and Castles, R. J. (1999). Flow limitation in uniform thick-walled collapsible tubes. *J. Fluid Struct.* **13**, 399-418.
Bertram, C. D. and Pedley, T. J. (1982). A mathematical model of unsteady collapsible tube behaviour. *J. Biomech.* **15**, 39-50.
Bertram, C. D., Raymond, C. J. and Pedley, T. J. (1990). Mapping of instabilities for flow through collapsible tubes of different length. *J. Fluid Struct.* **4**, 125-153.
Bertram, C. D., Raymond, C. J. and Pedley, T. J. (1991). Application of nonlinear dynamics concepts to the analysis of self-excited oscillations of a collapsible tube conveying a fluid. *J. Fluid Struct.* **5**, 391-426.
Bertram, C. D., Timmer, J., Müller, T. G., Maiwald, T., Winterhalder, M. and Voss, M. U. (2004). Aperiodic flow-induced oscillations of collapsible tubes: a critical reappraisal. *Med. Eng. Phys.* **26**, 201-214.
Brackenbury, J. H. (1972). Lung-air-sac anatomy and respiratory pressures in the bird. *J. Exp. Biol.* **57**, 543-550.
Brackenbury, J. H. (1979). Aeroacoustics of the vocal organs of birds. *J. Theor. Biol.* **81**, 341-349.
Brecher, G. A., Mixter, G. and Share, L. (1952). Dynamics of venous collapse in superior vena cava system. *Am. J. Physiol.* **171**, 194-203.
Brittan-Powell, E. F., Dooling, R. J., Larsen, O. N. and Heaton, J. T. (1997). Mechanisms of vocal production in budgerigars (*Melopsittacus undulatus*). *J. Acoust. Soc. Am.* **101**, 578-589.
Conrad, W. A. (1969). Pressure-flow relationships in collapsible tubes. *IEEE Trans. BioMed. Eng.* **6**, 284-295.
Daley, M. and Goller, F. (2004). Tracheal length changes during zebra finch song and their possible role in upper vocal tract filtering. *J. NeuroBiol.* **59**, 319-330.
Deverge, M., Pelorson, X., Vilain, C., Lagrée, P. Y., Chentouf, F., Willems, J. and Hirschberg, A. (2003). Influence of the collision on the flow through in-vitro rigid models of the vocal folds. *J. Acoust. Soc. Am.* **114**, 3354-3362.
De Vries, M. P., Van der Plaats, A., Van der Torn, M., Mahieu, H. F., Schutte, H. K. and Verkerke, G. J. (2000). Design and *in vitro* testing of a voice-producing element for laryngectomized patients. *Int. J. Artif. Organs* **23**, 462-472.
De Vries, M. P., Schutte, H. K., Veldman, A. E. P. and Verkerke, G. J. (2002). Glottal flow through a two-mass model: comparison of Navier-Stokes solutions with simplified models. *J. Acoust. Soc. Am.* **111**, 1847-1853.
De Vries, M. P., Hamburg, M. C., Schutte, H. K., Verkerke, G. J. and Veldman, A. E. P. (2003). Numerical simulation of self-sustained oscillation of a voice-producing element based on Navier-Stokes equations and the finite element method. *J. Acoust. Soc. Am.* **113**, 2077-2083.
Doupe, A. and Kuhl, P. (1999). Birdsong and human speech: common themes and mechanisms. *Annu. Rev. Neurosci.* **22**, 567-631.
Duncker, H. R. (1971). The lung air sac system of birds: a contribution to the functional anatomy of the respiratory apparatus. *Ergeb. Anat. Entwicklungsgesch.* **45**, 7-171.
Dürrwang, R. (1974). Funktionelle Biologie, Anatomie und Physiologie der Vogelstimme. PhD dissertation, University of Basel, Switzerland.
Elemans, C. P. H., Spierts, I. L. Y., Muller, U. K., van Leeuwen, J. L. and Goller, F. (2004). Superfast muscles control dove's trill. *Nature* **431**, 146.
Elemans, C. P. H., Spierts, I. L. Y., Hendriks, M., Schipper, H., Müller, U. K. and van Leeuwen, J. L. (2006). Syringeal muscles fit the trill in ring doves (*Streptopelia risoria* L.). *J. Exp. Biol.* **209**, 965-977.
Elemans, C. P. H., Zaccarelli, R. and Herzel, H. (2008a). Biomechanics and control of vocalization in a non-songbird. *J. R. Soc. Interface* **5**, 691-703.
Elemans, C. P. H., Mead, A. J., Rome, L. C. and Goller, F. (2008b). Superfast vocal muscles control sound production in songbirds. *PLoS ONE* **3**, e2581.
Ellington, C. P., van den Berg, C., Willmott, A. P. and Thomas, A. L. R. (1996). Leading-edge vortices in insect flight. *Nature* **384**, 626-630.
Eysholdt, U, Rosanowski, F. and Hoppe, U. (2003). Vocal fold vibration irregularities caused by different types of laryngeal asymmetry. *Eur. Arch. Otorhinolaryngol.* **260**, 412-417.
Fee, M. S. (2002). Measurement of the linear and nonlinear mechanical properties of the oscine syrinx: implications for function. *J. Comp. Physiol. A* **188**, 829-839.
Fee, M. S., Shraiman, B., Pesaran, B. and Mitra, P. P. (1998). The role of nonlinear dynamics of the syrinx in the vocalisations of a songbird. *Nature* **395**, 67-71.
Fitch, W. T. (1999). Acoustic exaggeration of size in birds by tracheal elongation: comparative and theoretical analysis. *J. Zool. Lond.* **248**, 31-49.
Fletcher, N. H. (1988). Bird song: a quantitative acoustic model. *J. Theor. Biol.* **135**, 455-481.
Fletcher, N. H., Riede, T., Beckers, G. J. L. and Suthers, R. A. (2005). Vocal tract filtering and the 'coo' of doves. *J. Acoust. Soc. Am.* **116**, 3750-3756.
Fletcher, N. H., Riede, T. and Suthers, R. A. (2006). Model for vocalization by a bird with distensible vocal cavity and open beak. *J. Acoust. Soc. Am.* **119**, 1005-1011.
Frank, T., Walter, I., Probst, A. and König, H. E. (2006). Histological aspects of the syrinx of the male mallard (*Anas plathyrhynchos*). *Anat. Histol. Embryol.* **35**, 396-401.
Gardner, T., Cecchi, G., Magnasco, M., Laje, R. and Mindlin, G. B. (2001). Simple motor gestures for birdsongs. *Phys. Rev. Lett.* **87**, 208101-208105.
Gaunt, A. S. (1983). An hypothesis concerning the relationship of syringeal structure to vocal abilities. *Auk* **100**, 853-862.
Gaunt, A. S., Gaunt, S. L. L. and Casey, R. M. (1982). Syringeal mechanisms reassessed: evidence from *Streptopelia*. *Auk* **99**, 474-494.
Goller, F. and Larsen, O. N. (1997a). *In situ* biomechanics of the syrinx and sound generation in pigeons. *J. Exp. Biol.* **200**, 2165-2176.
Goller, F. and Larsen, O. N. (1997b). A new mechanism of sound generation in songbirds. *Proc. Natl. Acad. Sci. USA* **94**, 14787-14791.
Goller, F. and Suthers, R. A. (1996a). Role of syringeal muscles in gating airflow and sound production in singing brown thrashers. *J. Neurophysiol.* **75**, 867-876.
Goller, F. and Suthers, R. A. (1996b). Role of syringeal muscles in controlling the phonology of bird song. *J. Neurophysiol.* **76**, 287-300.
Goller, F., Mallinckrodt, M. J. and Torti, S. D. (2004). Beak gape dynamics during song in the zebra finch. *J. Neurobiol.* **59**, 289-303.
Grotberg, J. B. and Jensen, O. E. (2004). Biofluid mechanics in flexible tubes. *Ann. Rev. Fluid Mech.* **36**, 121-147.
Hatzikirou, H., Fitch, W. T. and Herzel, H. (2006). Voice instabilities due to source-tract interactions. *Acta. Acust. Acust.* **92**, 468-475.
Hazel, A. L. and Heil, M. (2003). Steady finite-Reynolds-number flows in three-dimensional collapsible tubes. *J. Fluid Mech.* **486**, 79-103.
Heil, M. (1997). Stokes flow in collapsible tubes: computation and experiment. *J. Fluid Mech.* **353**, 285-312.
Herzel, H., Berry, D. A., Titze, I. R. and Saleh, M. (1994). Analysis of vocal disorders with methods from nonlinear dynamics. *J. Speech Hear. Res.* **37**, 1008-1019.
Herzel, H., Berry, D. A., Titze, I. R. and Steinecke, I. (1995). Nonlinear dynamics of the voice: signal analysis and biomechanical modeling. *Chaos* **5**, 30-34.
Hofmans, G. C. J., Groot, G., Ranucci, M., Graziani, G. and Hirschberg, A. (2003). Unsteady flow through in-vitro models of the glottis. *J. Acoust. Soc. Am.* **113**, 1658-1675.
Ishizaka, K. and Flanagan, J. L. (1972). Synthesis of voiced sounds from a two-mass model of the vocal cords. *Bell. Syst. Tech. J.* **51**, 1233-1268.
Jensen, K. K., Cooper, B. G., Larsen, O. N. and Goller, F. (2007). Songbirds use pulse tone register in two voices to generate low-frequency sound. *Proc. Biol. Sci.* **274**, 2703-2710.
Jensen, O. E. and Heil, M. (2003). High-frequency self-excited oscillations in a collapsible-channel flow. *J. Fluid Mech.* **481**, 235-268.
King, A. S. (1989). *Form and Function in Birds* (ed. A. S. King and J. McLelland), pp. 105-192. New York: Academic Press.
Kinsler, L. E., Frey, A. R., Coppens, A. B. and Sanders, J. V. (1982). *Fundamentals of Acoustics*, 3rd edn. New York: John Wiley.
Knowlton, F. P. and Starling, E. H. (1912). The influence of variations in temperature and blood-pressure on the performance of the isolated mammalian heart. *J. Physiol. Lond.* **44**, 206-219.
Koehl, M. A. R. (2006). Physical modelling in biomechanics. *Philos. Trans. R. Soc. B Biol. Sci.* **358**, 1589-1596.
Laje, R. and Mindlin, G. B. (2002). Diversity within a birdsong. *Phys. Rev. Lett.* **89**, 288102-288106.
Laje, R. and Mindlin, G. B. (2005a). Modelling source-source and source-filter acoustic interaction in birdsong. *Phys. Rev. Lett.* **2**, 036218.
Laje, R. and Mindlin, G. B. (2005b). *The Physics of Bird Song*. Berlin: Springer.
Laje, R., Gardner, T. J. and Mindlin, G. B. (2001). Continuous model for vocal fold oscillations to study the effect of feedback. *Phys. Rev. Lett.* **64**, 056201.
Laje, R., Gardner, T. J. and Mindlin, G. B. (2002). Neuromuscular control in vocalizations in birdsong: a model. *Phys. Rev. Lett.* **65**, 051921-051928.
Larsen, O. N. and Goller, F. (1999). Role of syringeal vibrations in birds vocalizations. *Proc. R. Soc. Lond. B* **266**, 1609-1615.
Larsen, O. N. and Goller, F. (2002). Direct observation of syringeal muscle function in songbirds and a parrot. *J. Exp. Biol.* **205**, 25-35.
Lucero, J. C. (1999). A theoretical study of the hysteresis phenomenon at vocal fold oscillation onset-offset. *J. Acoust. Soc. Am.* **105**, 423-431.

Luo, X. Y. and Pedley, T. J. (1996). A numerical simulation of unsteady flow in a two-dimensional collapsible channel *J. Fluid Mech.* **314**, 191-225.
Lyon, C. K., Scott, S. C., Anderson, D. K. and Wang, C. Y. (1981). Flow through collapsible tubes at high Reynolds numbers. *Circ. Res.* **49**, 988-996.
Marzo, A., Luo, X. Y. and Bertram, C. D. (2005). Three-dimensional collapse and steady flow in thick-walled flexible tubes. *J. Fluids Struct.* **20**, 817-835.
Mergell, P., Herzel, H. and Titze, I. (2000). Irregular vocal fold vibration: high-speed observation and modeling *J. Acoust. Soc. Am.* **108**, 2996-3002.
Miller, A. H. (1934). The vocal apparatus of some North American owls. *Condor* **36**, 204-213.
Mindlin, G. B., Gardner, T. J., Goller, F. and Suthers, R. A. (2003). Experimental support for a model of birdsong production. *Phys. Rev. E. Stat. Nonlin. Soft Matter Phys.* **68**, 041909.
Morse, P. M. (1948). *Vibration and Sound.* New York: American Institute of Physics.
Neubauer, J., Mergell, P., Eysholdt, U. and Herzel, H. (2001). Spatio-temporal analysis of irregular vocal fold oscillations: biphonation due to desynchronization of spatial modes. *J. Acoust. Soc. Am.* **110**, 3179-3192.
Nowicki, S. (1987). Vocal tract resonances in oscine bird sound production: evidence from birdsongs in a helium atmosphere. *Nature* **325**, 53-55.
Paulsen, K. (1967). *Das Prinzip der Stimmbildung in der Wirbeltierreihe und beim Menschen.* Frankfurt: Akademische Verlagsgesellschaft**.**
Pedley, T. J. and Luo, X. Y. (1998). Modelling flow and oscillations in collapsible tubes. *Theor. Comput. Fluid Dyn.* **10**, 277-294.
Percival, D. B. and Walden, A. T. (1993). *Spectral Analysis For Physical Applications: Multitaper and Conventional Univariate Techniques.* Cambridge: Cambridge University Press.
Riede, T., Suthers, R. A., Fletcher, N. H. and Blevins, W. E. (2006). Songbirds tune their vocal tract to the fundamental frequency of their song. *Proc. Natl. Acad. Sci. USA* **103**, 5543-5548.
Rüppel, W. (1933). Physiologie und Akustik der Vogelstimme. *J. Ornithol.* **81**, 433-542.
Ruty, N., Cisoni, J., Pelorson, X., van Hirtum, A., Lopez, I. and Hirschberg, A. (2007). An *in vitro* setup to test the relevance and the accuracy of low-order vocal fold models. *J. Acoust. Soc. Am.* **121**, 479-490.
Sane, S. P. and Dickinson, M. H. (2002). The aerodynamic effects of wing rotation and a revised quasi-steady model of flapping flight. *J. Exp. Biol.* **205**, 1087-1096.
Scala, G., Corona, M. and Pelagalli, G. V. (1990). Sur la structure de la syrinx chez le canard (*Anas platyrhinchos*). *Anat. Histol. Embryol.* **19**, 135-142.
Sciamarella, D. and d'Alessandro, C. (2004). On the acoustic sensitivity of a symmetrical two-mass model of the vocal folds to the variation of control parameters. *Acta Acust.* **90**, 746-761.
Seikel, J. A., King, D. W. and Drumright, D. G. (1997). *Anatomy and Physiology for Speech and Language.* San Diego, CA: Singular Publishing Group.
She, J. and Bertram, C. D. (1996). Numerical simulation of collapsible-tube flows with sinusoidal forced oscillation. *Bull. Math. Biol.* **58**, 1023-1946.
Suthers, R. A. (1990). Contributions to birdsong from the left and right sides of the intact syrinx. *Nature* **347**, 473-477.
Suthers, R. A., Narins, P. M., Lin, W. Y., Schnitzler, H., Denzinger, A., Xu, C. H. and Feng, A. S. (2006). Voices of the dead: complex nonlinear vocal signals from the larynx of an ultrasonic frog. *J. Exp. Biol.* **209**, 4984-4993.
Švec, J. G., Schutte, H. and Miller, D. G. (1996). A subharmonic vibratory patterns in normal vocal folds. *J. Speech Hear. Res.* **39**, 135-143.
Švec, J. G., Horáček, J., Šram, F. and Veselý, J. (2000). Resonance properties of the vocal folds. *J. Acoust. Soc. Am.* **108**, 1397-1407.
Tack, J. W., Verkerke, G. J., van der Houwen, E. B., Mahieu, H. F. and Schutte, H. K. (2006). Development of a double-membrane sound generator for application in a voice-producing element for laryngectomized patients. *Ann. Biomed. Eng.* **34**, 1896-1907.
Thompson, D. J. (1982). Spectrum estimate and harmonic analysis. *Proc. IEEE* **70**, 1055-1096.
Thompson, S. L., Mongeau, L. and Frankel, S. (2004). Aerodynamic transfer of energy to the vocal folds. *J. Acoust. Soc. Am.* **118**, 1689-1700.
Titze, I. R. (2002). *Principles of Voice Production.* Englewood Cliffs, NJ: Prentice-Hall.
Van Hirtum, A., Cisoni, N., Pelorson, X., Lopex, I. and Hirschberg, A. (2007). Experimental validation of some issues in lip and vocal fold physical models. *Acta Acust. Acust.* **93**, 314-323.
Vicario, D. S. (1991). Contributions of syringeal muscles to respiration and vocalization in the zebra finch. *J. Neurobiol.* **22**, 63-73.
Vincent, J. (1992). *Structural Biomaterials.* New York: Halsted Press.
Zaccarelli, R., Elemans, C. P. H., Fitch, W. T. and Herzel, H. (2006). Modelling bird songs: voice onset, overtones and registers. *Acta Acust. Acust.* **92**, 741-749.
Zhao, W., Zhang, C., Frankel, S. H. and Mongeau, L. (2002). Computational aeroacoustics of phonation, part I: Numerical methods, acoustic analogy validation, and effects of glottal geometry. *J. Acoust. Soc. Am.* **112**, 2134-2146.